Separation Science and Technology
Publication details, including instructions for authors and subscription information:
http://www.informaworld.com/smpp/title~content=t713708471

Modeling of Boehmite Leaching from Actual Hanford High-Level Waste Samples

R. A. Peterson[a]; G. J. Lumetta[a]; B. M. Rapko[a]; A. P. Poloski[a]
[a] Pacific Northwest National Laboratory, Richland, WA

To cite this Article Peterson, R. A. , Lumetta, G. J. , Rapko, B. M. and Poloski, A. P.(2007) 'Modeling of Boehmite Leaching from Actual Hanford High-Level Waste Samples', Separation Science and Technology, 42: 8, 1719 — 1730
To link to this Article: DOI: 10.1080/01496390701242111
URL: http://dx.doi.org/10.1080/01496390701242111

Separation Science and Technology, 42: 1719–1730, 2007

ISSN 0149-6395 print/1520-5754 online
DOI: 10.1080/01496390701242111

Modeling of Boehmite Leaching from Actual Hanford High-Level Waste Samples

R. A. Peterson, G. J. Lumetta, B. M. Rapko, and A. P. Poloski
Pacific Northwest National Laboratory, Richland, WA

Abstract: The Department of Energy plans to vitrify approximately 60,000 metric tons of high level waste sludge from underground storage tanks at the Hanford Nuclear Reservation. To reduce the volume of high level waste requiring treatment, a goal has been set to remove about 90 percent of the aluminum, which comprises nearly 70 percent of the sludge. Aluminum in the form of gibbsite and sodium aluminate can be easily dissolved by washing the waste stream with caustic, but boehmite, which comprises nearly half of the total aluminum, is more resistant to caustic dissolution, and requires higher treatment temperatures and hydroxide concentrations. In this work, the dissolution kinetics of aluminum species during caustic leaching of actual Hanford high level waste samples is examined. The experimental results are used to develop a shrinking platelet model that provides a basis for the prediction of dissolution dynamics from a known process temperature and hydroxide concentration. This model is further developed to include the effects of particle size polydispersity, which is found to strongly influence the rate of dissolution. Two identical parameters for this model are used to describe leaching data from two sets of leaching results. When compared to other common monodisperse shrinking particle models, this result suggests a more physically meaningful model.

Keywords: Boehmite, dissolution, high level waste

INTRODUCTION

Approximately 60,000 metric tons of high level waste (HLW) sludge are currently contained in 177 underground storage tanks at the Hanford

Received 3 October 2006, Accepted 27 December 2006
Address correspondence to R. A. Peterson, Pacific Northwest National Laboratory, 902 Battelle Blvd, Richland, WA 99354. E-mail: reid.peterson@pnl.gov

Nuclear Reservation in Richland, Washington. It is the intention of the U.S. Department of Energy to vitrify this sludge into a final glass waste form for storage in Yucca Mountain, Nevada. However, as much as 70 percent of this sludge is composed of aluminum. The Hanford Waste Treatment Plant (WTP) has a processing target to remove sufficient aluminum such that it is no longer the waste-limiting component in the final HLW glass wasteform. For the tank wastes considered in Fig. 1, the leaching process goal is to dissolve approximately 90% of the aluminum from the waste prior to vitrification.

The speciation of aluminum in the Hanford tank farm inventory is not fully quantified. However, nearly half of the high aluminum sludge boiled during storage due to fission product decay heat (1). This provides a thermal mechanism to convert gibbsite to boehmite in the Hanford tank farm (2, 3). Therefore, up to half of the Hanford sludge might be speciated as boehmite (while the balance is likely gibbsite and sodium aluminate with a small fraction of alumino-silicate) (4). The gibbsite and sodium aluminate will dissolve under relatively mild conditions (e.g. 8 hours at 50°C with 3 M NaOH) (5, 6). However, boehmite dissolution requires more aggressive hydroxide and temperature conditions and dissolves according to the reaction shown in equation (5, 6). As all the solids remaining after leaching will be processed as HLW, identifying the effect of process variables such as temperature and hydroxide concentration will allow better understanding

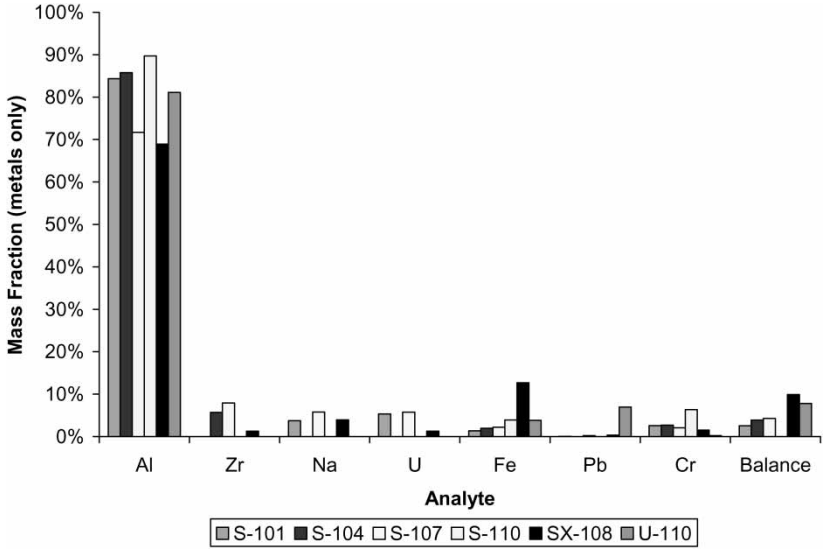

Figure 1. Insoluble metal content measured in selected high boehmite tanks.

of and control over the volume of solids requiring vitrification and, ultimately, the quantity HLW glass formed.

$$\mathrm{AlOOH} + \mathrm{OH^-} + \mathrm{H_2O} \longleftrightarrow \mathrm{Al(OH)_4^-} \tag{1}$$

To date, six separate actual waste dissolution studies have been performed with waste samples containing a significant fraction of boehmite (7–11). X-ray diffraction measurements for selected samples have confirmed that these samples contain predominantly boehmite. As seen in Fig. 1, the majority (70 to 90%) of the insoluble metal in these samples is aluminum. The purpose of this work was to identify a leaching model that appropriately describes the kinetic behavior of these six waste dissolution tests. This will help to determine the feasible hydroxide concentration and processing temperature conditions for boehmite leaching in the Hanford Waste Treatment Plant.

THEORY

Scotford et al. (5, 6) measured the kinetics of dissolution for boehmite at various temperatures and sodium hydroxide concentrations. They found that the reaction was half-order with respect to hydroxide concentration and followed an Arrehnius equation for temperature dependence. Skoufadis et al. (12) described the precipitation of boehmite as second order with respect to aluminate concentration. By starting with the reaction rate and equilibrium condition equations and by assuming a constant hydroxide concentration during leaching, the following relation for a reversible surface reaction is derived:

$$-\frac{dC_B}{dt} = k_s C_{OH}^{1/2}\left[1 - \left(\frac{C_{Al,o} + C_{Al,s}X_B}{C_{Al,e}}\right)^2\right] \tag{2}$$

$$k_s = Ae^{E/RT} \tag{3}$$

where

C_B = concentration of Boehmite on the particle surface (mol m^{-2})
k_s = surface reaction rate (mol$^{0.5}$ L$^{0.5}$ m^{-2} sec^{-1})
R = gas constant (8.314 J mol^{-1} K^{-1})
A = frequency factor (mol$^{0.5}$ L$^{0.5}$ m^{-2} sec^{-1})
E = Activation energy (123 kJ mol^{-1}) (5, 6)
T = reaction temperature (K)
C_{OH} = hydroxide concentration in the leach solution (mol L^{-1})
$C_{Al,o}$ = initial aluminate concentration (mol L^{-1})
$C_{Al,s}$ = initial molar quantity of boehmite in the solid phase per volume of leach solution (mol L^{-1})
$C_{Al,e}$ = aluminate concentration at equilibrium (mol L^{-1})
X_B = conversion of boehmite (mass fraction).

Dissolution of solid particulates has been successfully modeled with the shrinking core approach. Levenspiel (13) provides equations derived for film-diffusion, ash-diffusion, and surface-reaction-controlled regimes of differing particle shapes. Boehmite precipitates in platelet forms. Depending on the length of the platelet crystal, the particles are described as "lozenges" or "prisms." Scanning electron microscope images taken of particles from the Hanford tank farm (14) (see Fig. 2) indicate that the boehmite exists as a distribution of lozenge-shaped particles. The length of the boehmite particles is approximately 100 nm.

In a simplistic model, the growth of these crystals is assumed to be linear with the growth surface on a crystal plane. Dissolution is expected to simply reverse this process, resulting in a decreasing crystal length as a function of time. This situation describes the flat-plate dissolution model presented by Levenspiel (13). With the high activation energy and long leaching time required, the surface-reaction-controlled regime is expected to dominate the kinetics of the process. This is confirmed by calculation of the Damkohler number (ratio of reaction to diffusion rates) using typical values for the diffusivity of hydroxide ions in water. The Damkohler number was determined to be on the order of 10^{-9} to 10^{-7}. This indicates that particle sizes on the order of meters are needed to result in diffusion limited kinetics. The equations describing the kinetics of the surface reaction dominated regime is:

$$\frac{dX_B}{dt} = \frac{k_s C_{OH}^{1/2}}{\rho_B L}\left[1 - \left(\frac{C_{al,o} + C_{Al,s}X_B}{C_{Al,e}}\right)^2\right] \tag{4}$$

where X_B is the boehmite conversion, t is the dissolution time, ρ_B is the molar density of boehmite (50,500 mol m^{-3}) (5, 6), and L is the initial particle length (m^{-1}). If the initial concentration of aluminate is

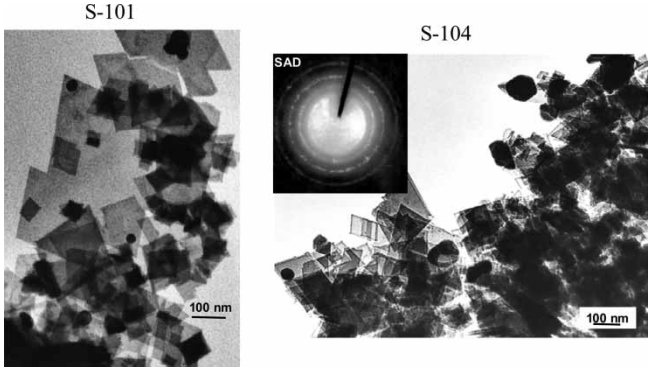

Figure 2. Boehmite phases in untreated S-101 and S-104 solids (10).

assumed zero, Eq. (4) can be solved analytically:

$$X_B = \frac{C_{Al,e}}{C_{Al,s}} \tanh\left(\frac{k_s C_{OH}^{1/2} C_{Al,s}}{\rho_B L C_{Al,e}} t\right) \tag{5}$$

Levenspiel (13) describes the surface reaction-controlled dissolution of other particle shapes, including cylindrical and spherical shaped particles through equations (6) and (7), respectively.

$$\frac{dX_B}{dt} = \frac{4k_s C_{OH}^{1/2}}{\rho_B D}(1 - X_B)^{1/2}\left[1 - \left(\frac{C_{Al,o} + C_{Al,s}X_B}{C_{Al,e}}\right)^2\right] \tag{6}$$

$$\frac{dX_B}{dt} = \frac{6k_s C_{OH}^{1/2}}{\rho_B D}(1 - X_B)^{2/3}\left[1 - \left(\frac{C_{Al,o} + C_{Al,s}X_B}{C_{Al,e}}\right)^2\right] \tag{7}$$

where D is the initial particle diameter (m^{-1}).

Gbor et al. (15) observed that the above equations are based on a monodisperse particle size distribution. Despite this limitation, these monodisperse diffusion-controlled models were still able to capture surface-controlled reaction kinetics in applications where a distribution of particles was present. One difficulty was that surface-controlled dissolution dynamics for polydisperse platelet particles could only be properly captured by treating them as mono-sized spheres. To correct this problem, Gbor extended the shrinking particle models to particle size distributions typically observed in practice through the use of the Gamma distribution. The equations describing the Gamma distribution are shown below:

$$p(L) = \frac{1}{\beta^\alpha \Gamma(\alpha)} L^{\alpha-1} e^{L/\beta} \tag{8}$$

$$\mu = \alpha\beta \tag{9}$$

$$\sigma = \alpha^{0.5}\beta \tag{10}$$

where *p(L)* is the probability function for a flat plate particle with a distance between actively dissolving surfaces L, Γ is the Gamma function, α and β are positive parameters, μ is the mean value of the distribution, and σ is the standard deviation.

The overall conversion for a distribution of particles, X_B^*, is given in the equations below:

$$X_B^* = 1 - \int_{L_s}^{L_{\max}} f(L, t)p(L)dL \tag{11}$$

$$f(L, t) = 1 - X_B \tag{12}$$

Combining Equations (5), (8), (11), and (12) produces an equation describing the dissolution of boehmite based on a model system of a distribution of

various length shrinking platelets.

$$X_B^* = 1 - \int_{L_s}^{L_{\max}} \left[1 - \frac{C_{Al,e}}{C_{Al,s}} \tanh\left(\frac{k_s C_{OH}^{1/2} C_{Al,s}}{\rho_B L C_{Al,e}} t \right) \right] \times \frac{1}{\beta^\alpha \Gamma(\alpha)} L^{\alpha-1} e^{L/\beta} dL \quad (13)$$

In this equation, L_{max} is the maximum length of the initial undissolved plates; L_t is the largest particle completely dissolved at time, t, and is given as follows:

$$L_t = \frac{k_s C_{OH}^{1/2} C_{Al,s}}{\rho_B C_{Al,e} \tanh(C_{Al,s}/C_{Al,e})} t \quad (14)$$

As Gbor et al. (15) states, L_{max} should be chosen such that at least 99.9% of the particle volume in the distribution is mathematically considered. For the modeling results presented in this work, L_{max} was set to 10 μm, which meets the criterion shown below:

$$\int_0^{L_{\max}} \frac{1}{\beta^\alpha \Gamma(\alpha)} L^{\alpha-1} e^{L/\beta} dL \geq 0.999 \quad (15)$$

TESTING

Initial dissolution tests involved mixing the insoluble sludge samples with a quantity of 2 to 5 M NaOH. These tests involved relatively short (4 to 5 hour) contacts. Table 1 summarizes the processing conditions and leaching results from these short contact time tests. All of these tests were performed at 100°C (with the exception of the S-101 tests at 2.6 M NaOH, which was

Table 1. Conditions and results from short duration tests

Sample	C_{OH} (mol/L)	Test duration (hr)	Median particle diameter (μm)	$C_{Al,s}$ (mol/L)	$C_{Al,e}$ (mol/L)	X_B
S-101	2.6	5	6.8	0.6	0.5	0.28
S-101	4.7	5	6.8	2.3	1.0	0.11
S-104	3.6	5	23.2	0.6	0.7	0.39
S-104	4.8	5	23.2	6.9	1.0	0.10
S-107	3.1	5	12.8	0.8	0.6	0.56
S-110	3.0	4	nm	0.2	0.6	0.23
SX-108	3.7	5	25.7	0.7	0.7	0.28
U-110	2.6	5	33.0	1.0	0.5	0.37

nm- not measured.

performed at 95°C). Additional information, such as experimental methods and materials used in the course of these tests, may be found in Ref. (7–11)

Inspection of Table 1 shows that a wide range of dissolution performance was observed between samples from different tanks. Boehmite solubility as a function of temperature and hydroxide concentration is provided from Panias et al. (16) Several data points appear to represent systems that are likely slowed by aluminum solubility limitations. Unfortunately, no clear trend in the dissolution rate is observed with a single measurement point at 5 hours dissolution time. To better understand the mechanisms governing the leaching performance, a second series of dissolution tests, reported in Ref. (7, 11), were performed with samples from Hanford tanks S-110 and S-101. These tests involved periodically measuring the dissolution over longer durations with a broader range of hydroxide concentrations. Table 2 provides the conditions for these tests.

RESULTS

The surface-reaction-controlled equation for platelet particles equation (5) was numerically solved and plotted with boehmite conversion data for tanks S-101 and S-110 in Fig. 3. Implicit in these calculations is the assumption of mono-sized platelets. The frequency factor, A, is dependent on the actual portion of the particle surface area that is reacting. Because this area is unknown, the particle length initial condition was held constant at 100 nm, leaving the frequency factor as the only adjustable parameter. As seen in Fig. 3, the best-fit lines for equation (5) exhibit much slower dissolution than experimentally observed and, as such, do not adequately capture the measured kinetic data.

The dissolution kinetics were also compared against predictions made using the cylindrical and spherical particle models, given by equations (6) and (7), respectively. These two equations were solved in the same manner as the platelet model: the particle length initial condition was held constant at 100 nm and the frequency factor was treated as an adjustable parameter. Figures 4 and 5 show the resulting plots of the actual data and the best fit cylindrical and spherical particle model predictions. The fitted curves are

Table 2. Conditions for longer duration tests

Sample	C_{OH} (mol/L)	Duration (hr)	Temp (°C)	$C_{Al,s}$ (mol/L)	$C_{Al,e}$ (mol/L)
S-110	0.8	168	100	0.2	0.2
S-110	2.7	168	100	0.2	0.5
S-110	4.5	168	100	0.2	1.0
S-101	1.0	168	95	0.2	0.2
S-101	2.6	168	95	0.6	0.6

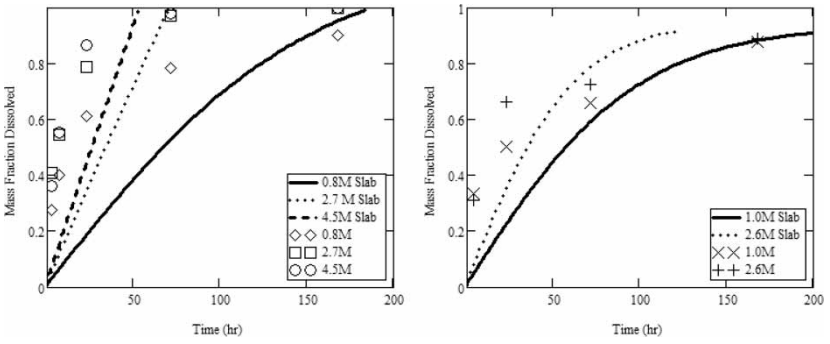

Figure 3. Dissolution curves for S-110 (left; $A = 2.1 \times 10^9$ $mol^{0.5}$ $L^{0.5}$ m^{-2} sec^{-1}; $r^2 = 0.38$) and S-101 (right; $A = 3.9 \times 10^9$ $mol^{0.5}$ $L^{0.5}$ m^{-2} sec^{-1}; $r^2 = 0.83$) for surface-reaction-controlled regimes of monodisperse platelet particles.

improved over the platelet model insofar as they tend to better predict the rapidness of dissolution. The spherical model clearly provides the best fit of the three surface reaction limited models considered thus far. While this may appear to conflict with results from direct microscopic examination of the waste samples (Fig. 2), a distribution of different platelet sizes can lead to an apparent spherical functionality. The success of the spherical model is most likely a result in the deficient treatment of platelet polydispersity. The disparity being particle geometries inferred from modeling and those observed directly might also result from the assumption of reaction-limited dissolution kinetics. Specifically, the models considered herein are based on the premise that diffusion-controlled dissolution mechanisms are not expected because of the relatively large activation energy and leach times required for dissolution. To confirm this assertion, diffusion controlled

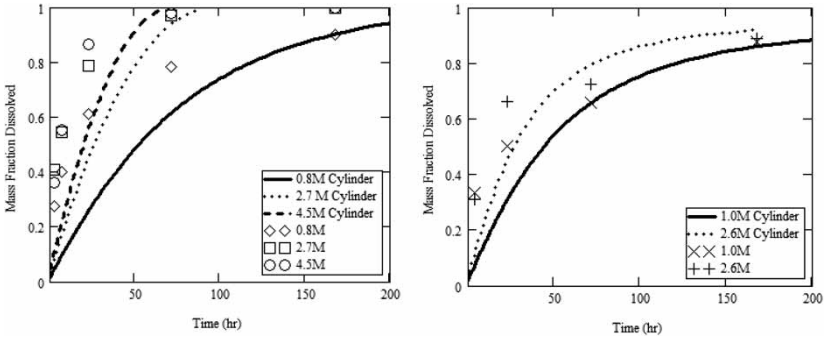

Figure 4. Dissolution curves for S-110 (left; $A = 7.9 \times 10^8$ $mol^{0.5}$ $L^{0.5}$ m^{-2} sec^{-1}; $r^2 = 0.64$) and S 101 (right; $A = 1.5 \times 10^9$ $mol^{0.5}$ $L^{0.5}$ m^{-2} sec^{-1}; $r^2 = 0.88$) for surface reaction controlled regimes of monodisperse cylindrical particles.

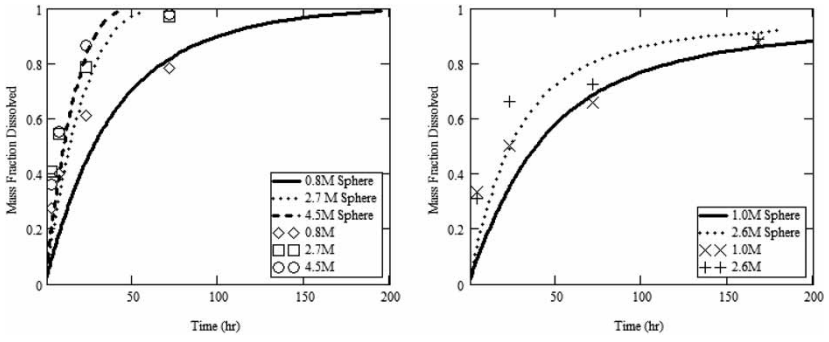

Figure 5. Dissolution curves for S-110 (left; $A = 1.1 \times 10^9$ $mol^{0.5}$ $L^{0.5}$ m^{-2} sec^{-1}; $r^2 = 0.79$) and S-101 (right; $A = 1.2 \times 10^9$ $mol^{0.5}$ $L^{0.5}$ m^{-2} sec^{-1}; $R^2 = 0.89$) for surface reaction controlled regimes of monodisperse spherical particles.

models for plate, cylinder, and sphere particles described by Levenspiel (13) were also performed, No suitable model was found.

The need to account for this polydisperisty is made apparent by the inability of surface reaction- and diffusion-limited models to appropriately capture dissolution dynamics when mono-sized platelets are assumed and by the apparent success of the spherical particle model. Equation (13), which is the extension of the particle size distribution model described by Gbor to plate-shaped particles, was numerically solved at experimental conditions with the mean value of the particle size distribution set at 100 nm. The results shown in Fig. 6 indicate a good fit between the model based on

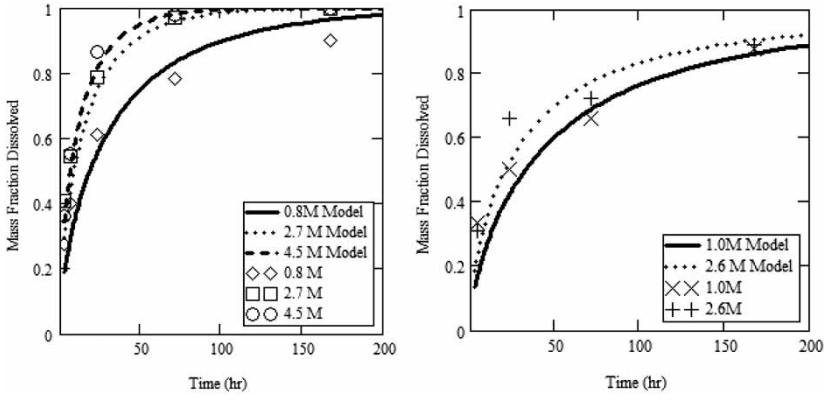

Figure 6. Dissolution curves for S-110 (left; $A = 4 \times 10^9$ $mol^{0.5}$ $L^{0.5}$ m^{-2} sec^{-1}; $r^2 = 0.98$) and S-101 (right; $A = 4 \times 10^9$ $mol^{0.5}$ $L^{0.5}$ m^{-2} sec^{-1}; $r^2 = 0.96$) with model fits from equation 13.

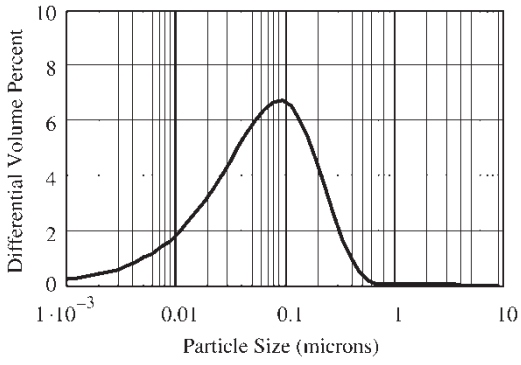

Figure 7. Particle size distributions used to obtain the leaching results shown in Fig. 6.

particle size distribution and the experimental data. In this model, the mean value of the particle size distribution, μ, was held constant at 100 nm, and two adjustable parameters were used, α and A. Since the mean value of the particle size distribution is set to a constant value, the standard deviation of the distribution is specified only by the variable, α, as shown by equations (9) and (10). In both cases, the optimal value of α was found to be unity which results in a 100 nm standard deviation for the particle size distribution. Additonally, the optimal value of A was found to be 4×10^9 mol$^{0.5}$ L$^{0.5}$ m^{-2} for both S-101 and S-110. Literature values were used for the remainder of the model parameters (see Theory section for more details), including reaction order (half order with respect to hydroxide concentration and second order with respect to aluminate concentration) and activation energy (E = activation energy (123 kJ mol^{-1}) from Scotford (5, 6). Note that the model results for both tanks (S-101 and S-110) use the identical values for the frequency factor, A, and the particle size distribution shown in Fig. 7.

The frequency factor and particle size distribution parameters for the polydisperse model were solved independently for tanks S-101 and S-110 and were found to be identical (see Fig. 6). This is compared to the spherical model (see Fig. 5) results that had a 10% difference in frequency factor between tank leaching results with marginal correlation coefficients. The fact that a single pair of parameters for the polydisperse model describes separate leaching results across multiple tanks with high correlation coefficients suggests that this model is physically meaningful.

CONCLUSIONS

Boehmite dissolution data were analyzed from several actual waste samples. In particular, data from S-101 and S-110 were analyzed to determine the most

appropriate reaction model. Data analysis indicates that a model described by Gbor et al. (15) provided a satisfactory fit to the experimental data. The Gbor model considers solid/fluid reactions over a range of particle sizes and was extended from spherical- to platelet-shaped particles. Particle size distributions calculated from the platelet-based model agreed well with experimental data. These results provide a basis for prediction of dissolution dynamics from known process temperature and hydroxide concentration. They also demonstrate the importance of having knowledge of the size distribution and morphology of the boehmite particles in contact with the caustic solution, as both significantly impact the rate of dissolution.

REFERENCES

1. Meacham, J.M. (2003) *Aluminum Wash and Leach Factors*: RPP-11079 Rev 0, CH2MHILL Hanford Group.
2. Martino, C.J. and Fondeur, F.F. (2002) *Gibbsite/Bayerite and Uranium in Tank 41H*; Westinghouse Savannah River Company: Aiken, SC29808, WSRC-RP-2002-00530.
3. Wefers, K. and Misra, C. (1987) *Oxides and Hydroxides of Aluminum*: Alcoa Technical Paper No. 19, Revised, Alcoa Laboratories: Pittsburgh, PA.
4. Rapko, B.M. and Lumetta, G.J. (2000) *Status Report on Phase Identification in Hanford Tank Sludges*; PNNL-13394.
5. Scotford, R.F. and Glastonb, Jr. (1971) Effect of temperature on rates of dissolution of gibbsite and boehmiite. *Canadian J. Chem. Eng.*, 49 (5): 611.
6. Scotford, R.F. and Glastonb, Jr. (1972) Effect of concentration on rates of dissolution of gibbsite and boehmite. *Canadian J. Chem. Eng.*, 50 (6): 754–758.
7. Lumetta, G.J. et al. (2001) *Caustic Leaching of Hanford Tank S-110 Sludge*, PNNL-13702, Pacific Northwest National Laboratory: Richland, WA.
8. Lumetta, G.J. et al. (1997) *Washing and Leaching of Hanford Tank Sludge: Results of FY1997 Studies*; PNNL-11636, Pacific Northwest National Laboratory: Richland, WA.
9. Lumetta, G.J. et al. (1996) *Washing and Caustic Leaching of Hanford Tank Sludges: Results of FY 1996 Studies*; PNNL-11278, Pacific Northwest National Laboratory: Richland, WA.
10. Lumetta, G.J. and Rapko, B.M. (1994) *Washing and Alkaline Leaching of Hanford Tank Sludges: A Status Report*, PNL-10078, Pacific Northwest National Laboratory: Richland, WA.
11. Lumetta, G.J., Rapko, B.M., and Liu, J. (1998) *Washing and Caustic Leaching of Hanford Tank Sludge: Results of FY 1998 Studies*; PNNL-12026, Pacific Northwest National Laboratory: Richland, WA.
12. Skoufadis, C., Panias, D., and Paspaliaris, I. (2003) Kinetics of boehmite precipitation from supersaturated sodium aluminate solutions. *Hydrometallurgy*, 60 (68): 57–68.
13. Levenspiel, O. (1999) *Chemical Reaction Engineering*, 3rd Edn.; Wiley: New York.
14. Lumetta, G.J., Rapko, B.M., Liu, J., and Temer, D.J. (1998) Enhanced sludge washing for pretreating hanford tank sludges. In *Science and Technology for*

Disposal of Radioactive Tank Wastes; Schulz, W.W. and Lombardo, N.J. (eds.); Plenum Press: New York, 203–218.
15. Gbor, P.K. and Jia, C.Q. (2004) Critical evaluation of coupling particle size distribution with the shrinking core model. *Chem. Eng. Sci.*, 59: 1979–1987.
16. Panias, D., Asimidis, P., and Paspaliaris, I. (2001) Solubility of boehmite in concentrated sodium hydroxide solutions: model development and assessment. *Hydrometallurgy*, 59: 15–29.